Received: 19 November 2020 | Revised: 8 July 2021 | Accepted: 7 September 2021

DOI: 10.1002/stc.2855

RESEARCH ARTICLE

WILEY

Detection of setting time in cement hydration using patch antenna sensor

Zhuoran Yi[1] | **Songtao Xue**[1,2] | **Liyu Xie**[1] | **Guochun Wan**[3]

[1]Department of Disaster Mitigation for Structures, Tongji University, Shanghai, China

[2]Department of Architecture, Tohoku Institute of Technology, Sendai, Japan

[3]Department of Electronic Science and Technology, Tongji University, Shanghai, China

Correspondence
Liyu Xie, Department of Disaster Mitigation for Structures, Tongji University, Shanghai, China.
Email: liyuxie@tongji.edu.cn

Funding information
National Natural Science Foundation of China, Grant/Award Numbers: 52078375, 52178298; the Key Laboratory of Performance Evolution and Control for Engineering Structures (Tongji University), the Ministry of Education of the People's Republic of China, Grant/Award Number: 2018KF-4

Summary

The dielectric constant of cement will decrease with an increase of moisture content, resulting in an increasing fundamental resonant frequency of a covered patch antenna. Based on this principle, the authors utilized a patch-antenna sensor to determine the initial and final setting time of cement during hydration by sensing the variation of moisture content. The theory of an equivalent dielectric constant model was adopted to exhibit the relationship between the fundamental resonant frequency of a buried antenna sensor and a dielectric constant in the covering cement paste. The phenomenon is then verified by both simulation in a high frequency structure simulator (HFSS) and experiments. The initial setting time of cement is regarded as the moment when the moisture content starts to increase rapidly and the final setting time is taken as the maximum moisture content acceleration. The setting times measured by the patch antenna sensor are compared with the results of the penetration resistance method using a Vicat apparatus with a testing error of less than 10%. A moisture content detection experiment was further carried out after the paste's hydration assuming the specimen was soaked in water. The results indicate that the resonant frequency of the patch antenna sensor is sensitive to moisture content change as fine as 4‰ with respect to the paste volume after cement hardening. The buried antenna sensor can detect the setting time during cement hydration and serve as a leakage detection sensor in service.

KEYWORDS

cement hydration, leakage detection, moisture content detection, patch antenna sensor, setting time, structural health monitoring

1 | INTRODUCTION

In these modern times, concrete remains an irreplaceable building material in civil engineering, supporting innumerable infrastructures from bridges to power plants.[1–3] As a composite material, it is composed of aggregates, water, and cement with well-calculated proportions. The stone-like product is then obtained through the hardening process due to the chemical reaction between cement and water, also called setting. Different kinds of admixtures can be intermixed to achieve high-strength or high-performance concrete for special uses or requirements.[4–6]

To ensure the safety and durability of concrete, it is important to periodically survey the strength and state of the concrete during and after construction, which to a great extent depends on the thoroughness of cement hydration for ordinary concrete and high-strength concrete.[7–10] According to Lootens and Bentz,[11] the early-age compressive strength changes almost linearly with the hydration progress, which can be investigated by the concrete setting state. Setting time is a significant aspect for the early-age constructing process, which has been specified in many building codes, such as those covering curing[12] and watertightness.[13] With the knowledge of setting time, the time for handling, transporting, placing and providing the required shape of concrete can be well organized for quality control. Hence, it is necessary to monitor the setting time of cement hydration during placing for compressive strength evaluation of early-age concrete.[14]

Conventionally, the setting time of cement is monitored by a penetration resistance method such as that made possible by the Vicat apparatus, which has been selected as the standard schema in European building code EN196-3-2016.[15] According to the code, for ordinary Portland concrete, the initial setting time is regarded as the time when the cement loses its plasticity, which is based on when the penetration resistance is first achieved at 3.4 MPa. The final setting time is deemed as the time when the cement has sufficient strength with a penetration resistance of 27.6 MPa. The setting time obtained from the penetration method is accurate enough for practical use, however, it requires skilled workers to test continuously for up to 8 h. Besides, the result obtained from the penetration method depends on the sample's surface flatness, which will be inaccurate for the concrete lying deeper inside.

To eliminate concrete setting time problems, various testing method have been developed. Koo et al,[16,17] proposed a testing method by analyzing the change of temperature induced by cement hydration. It is easy enough for the setting time measurement; however, in most cases the temperature shift is smaller than 10°C. Thus, the results are easily influenced by the daily temperature change especially diurnal temperature variation. Kong et al[18,19] designed an ultrasonic-wave-based setting time monitoring system. Because the characteristics of the stress wave propagation (such as power spectrum) highly depend on medium properties, the frequency domain analysis of both compressive wave (P-wave) and shear wave (S-wave) velocities can be utilized to study the very early age cement hydration progress. This analysis uses cables to supply power and transmit data, which is time- and labor- consuming due to the periodic manual inspections and cable deployment. In addition, the ultrasonic-wave-based monitoring system cost more than the penetration method. Thus, an urgent need exists to develop a cost-effective, portable system to monitor hydration and determine the initial and final setting time.

Analyzing the electrical properties of cement during hydration, has led to the development of some low-cost hydration sensors were proposed. Kazi et al.[14,20,21] proposed a low-cost setting time measurement system based on the transformer principle with a lossy capacitive load. The cement placed between two parallel metal plates behaves as a lossy dielectric, and the primary current in the cable changes with the process of cement hydration. Manchiryal et al.[22,23] developed a dielectric-response-based sensor for cement hydration. The variation in the conductivity of fresh cement during hydration was investigated to determine the setting time of cement. These sensors are inexpensive and easy to manufacture. However, these buried sensors are inconvenient for practical use due to the troublesome deployment of cables; moreover, a passive sensor without power and data cables for hydration process is more desirable for embedded concrete monitoring. Patch antenna sensor is verified to be effective for the moisture detection.[24–26] However, previous research did not apply it for the setting time sensing of cement or concrete. Besides, these patch antenna sensors mainly use the reflection coefficient as the sensing parameters, which is unstable when applied to the practical utilization.[27,28]

This paper utilizes a rectangular patch antenna sensor as a passive, wireless, and low-cost cement setting time sensing system. The dielectric constant of cement paste will decrease with the process of hydration.[29] Since the equivalent dielectric constant of the dielectric board in the patch antenna will increase due to the covering material with a high dielectric constant,[30–34] the resonant frequency shifts of an embedded patch antenna could reflect a hydration rate and further determine the setting time of covering cement paste. The resonant frequency of a patch antenna can be measured by a backscattering system.[34,35] This passive sensing system can be adopted for massive and distributed deployment of large-scale infrastructures.[36–38] During the service stage of concrete material after hardening, the proposed patch antenna sensor can be also used to monitor the moisture content of hardened cement and further predict leakage due to the sensitivity of the cement's dielectric constant to moisture content, which is useful for underwater concrete structure[39] and concrete dam.[40]

This paper is organized as follows. Section 2 introduces the concept of a setting time sensor based on a rectangular patch antenna. The resonant frequency of a rectangular patch antenna influenced by covering cement paste is calculated theoretically to show the sensing mechanism. We then determine the basic parameters for the patch antenna sensor. In Section 3, the sensing mechanism is further tested by simulation in a high frequency HFSS. Section 4 describes

the fabrication of sensors and the instrumentation setup of the experiments. Setting times are monitored and moisture content is detected after hardening to verify the performance of the proposed antenna sensor. Conclusions are then drawn, and future research potential is discussed.

2 | SENSING MECHANISM

A typical rectangular patch antenna consists of a ground plane, a substrate, and a radiation patch, as shown in Figure 1. Because the radiation parameters (especially scatter parameters) are affected by the physical dimension of the antenna and the humidity/temperature of the placing environment, the rectangular patch antenna has been used for wireless sensing and data transmission in structural health monitoring[41,42] with the advantage of low-cost, low-profile, conformable properties, and easy fabrication. A rectangular patch antenna sensor was installed on the surface to sense the quadric stress[36,43] and cracks.[44–47] The sensor can also be embedded in a structure to monitor humidity[48,49] or temperature.[50] In general, the dielectric constant of cement will be changed by the degree of moisture content, which further shifts the resonant frequencies of the built-in patch antenna. Therefore, the fundamental resonant frequency shifts could be utilized to present the degree of moisture content and determine the setting time of cement paste.

Since the patch antenna can be utilized to monitor the stress and temperature of attached structure simultaneously,[51] the temperature effect should also be investigated when the sensor is designed for humidity sensing. According to previous research, the temperature differences caused by concrete hydration is about 40°C in an adiabatic test.[10] Since the fundamental resonant frequency shift caused by temperature change (2 MHz/40°C) is much smaller than the shift caused by the variation of moisture content (about 40 MHz during early-age hydration),[49,50] the effect of temperature change is trivial in the antenna sensor design for sensing the setting time. Therefore, the moisture content effect on the embedded patch antenna is discussed in this paper, ignoring the temperature variation, and the setting time of the cement paste is obtained from the change rate of moisture content surrounding the patch during cement hydration.

2.1 | Relationship between moisture content and setting time

The water inside the fresh cement paste exists as free state and gel state, which should be both considered in the moisture content investigation. Generally speaking, the total amount of water inside the fresh cement paste will decrease with the hydration, which is shown in Figure 2. The reason for losing the free water is due to evaporation and hydration. According to Xu's survey,[53] the evaporation rate of free water keeps nearly constant during hydration.

Free water in fresh cement paste will participate in the hydration of cement (mainly for Ca_3SiO_5 [C_3S] very early in the process) and part of the free water will be transformed into gel water in the micro-pores around the cement gel, which is shown in Equation 91.

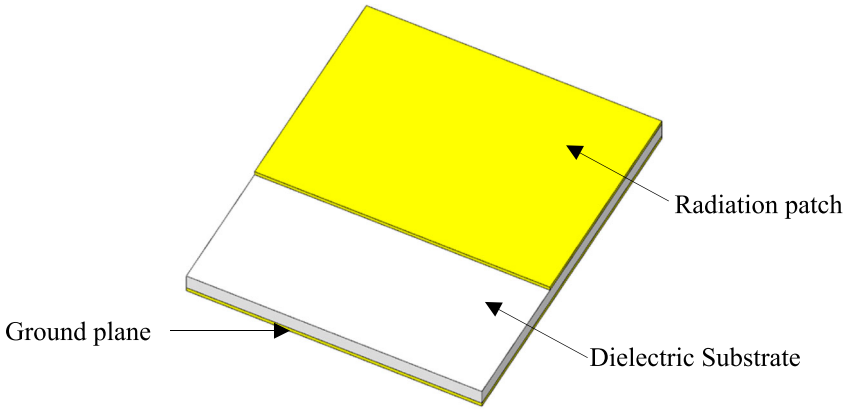

FIGURE 1 Concept figure of a normal rectangular patch antenna

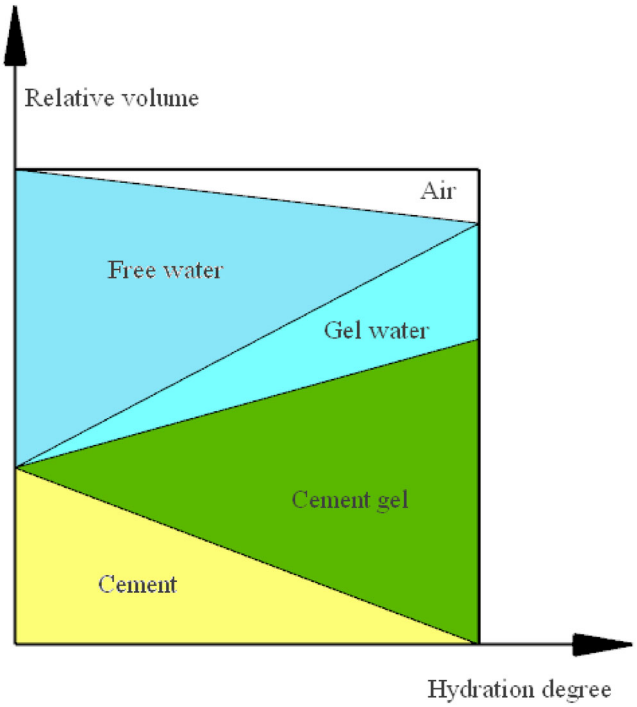

FIGURE 2 Change of free water and gel water inside cement paste during hydration[52]

$$Ca_3SiO_5 + (3+y-x)H_2O \rightarrow (CaO)_x(SiO_2)(H_2O)_y + (3-x)Ca(OH)_2 \quad (1)$$

where $(CaO)_x(SiO_2)(H_2O)_y$ is referred to as C–S–H gel.

When hydration is fully reached, the menisci are no longer present because all the free water has reacted with Portland cement.[52]

The cement hydration has several stages with different hydration rates. Taylor et al[54] has divided the early cement hydration into the initial hydrolysis period, induction period, acceleration period, deceleration period. The initial hydrolysis period happens after Portland cement and water are intermixed. The cement and water react violently, and soon the reaction declines. Free water is consumed rapidly during this period. Then the cement paste enters into an induction period. The hydration nearly ceases due to the formation of a protective layer in the surface of cement particles. The amount of free water will be affected mainly by evaporation during induction period. The induction period proceeds until the cement achieves its initial setting. During this period, the protective layer on the surface of a cement particle is dissolved and the cement will fully lose its plasticity. Cement hydration then enters into the acceleration period and speeds up again.

With Portland cement as an example, the change of total water testing from actual measurement during the hydration is shown in Figure 3.[55] Stage I refers to the initial hydrolysis and induction period. Stage II refers to acceleration period, and Stage III refers to the deceleration period. The end of the induction period is the initial setting of cement, and the final setting happens in the middle of the acceleration period due to the large generation of C–S–H gels, which is consuming large amounts of C_3S. Because the rate of hydration in the acceleration period is mainly determined by the quantity of C_3S, the hydration rate after the final setting will decrease. Based on the hydration process, the moment of maximum hydration rate (or the maximum change rate of the moisture content) is regarded as the final setting time of cement paste in this paper.

Moisture content varies due to hydration and water evaporation. As the evaporation rate keeps constant during hydration,[54] the acceleration of moisture content (the second order derivative of the moisture content with respect to time) can neutralize the interference brought by evaporation. Additionally, the variations in moisture content acceleration are able to represent the state of setting due to hydration. The maximum acceleration is considered the moment when the cement reaches its final setting time.

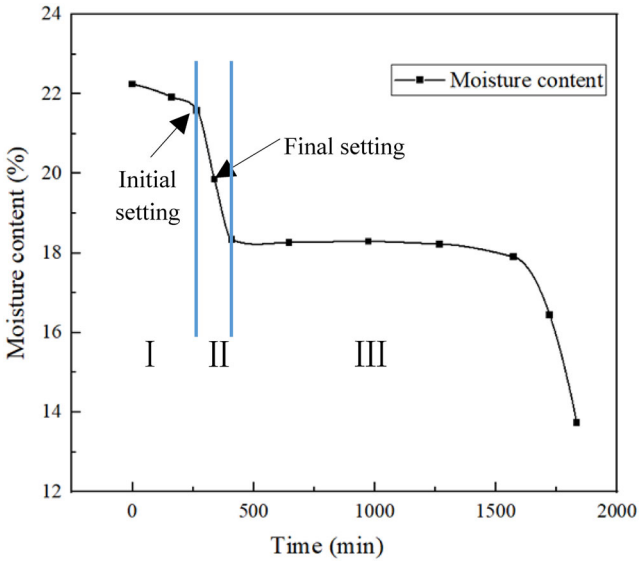

FIGURE 3 Relationship between moisture content and time during hydration[55]

Taking moisture content and change rate of moisture content as $f(t)$ and $g(t)$, $g(t)$ is the first order derivative of $f(t)$ with respect to time. Then, the initial setting time is when $f(t)$ starts to decrease rapidly and can be identified from the moisture content figure. The final setting time t_{fin} is the time when $g(t)$ reaches its maximum value and can be expressed as follows:

$$g(t) = f'(t) \tag{2}$$

$$g(t_{fin}) > g(t_{fin} \pm \Delta t) \quad \Delta t \in R \tag{3}$$

2.2 | Relationship between early-age concrete strength and setting time

Didier[11] defined the relationship between early-age concrete strength and concrete hydration. During the hydration progress, bridges made by hydration products are built between the cement clinker particles and then transform the cement paste from a viscous suspension to a rigid load-bearing solid (especially the C–S–H gel noted in early-age hydration), which further increases the early-age concrete strength. For ordinary Portland cement, a typical relationship between time and concrete strength is shown in Figure 4.[11]

In general, concrete starts to gain compressive strength at the initial setting and achieves 0.2–1 MPa at the final setting. The concrete will lose flowability and be prone to cracking after the initial setting, so that the continuous construction of columns, beams and slabs is required to be completed before initial setting. Furthermore, because the concrete before final setting lacks the strength to withstand bearing pressure, the concrete before the final setting cannot bear pressure.

2.3 | Relationship between the moisture content and dielectric constant of cement

The dielectric constant of a composite material can be calculated by Birchack's theory.[56–58] Therefore, the dielectric constant of fresh cement paste can be calculated by Equation 4 as:

$$K^{\alpha} = f_1 K_{fw}^{\alpha} + f_2 K_{cw}^{\alpha} + f_3 K_{solid}^{\alpha} + f_4 K_{air}^{\alpha} \tag{4}$$

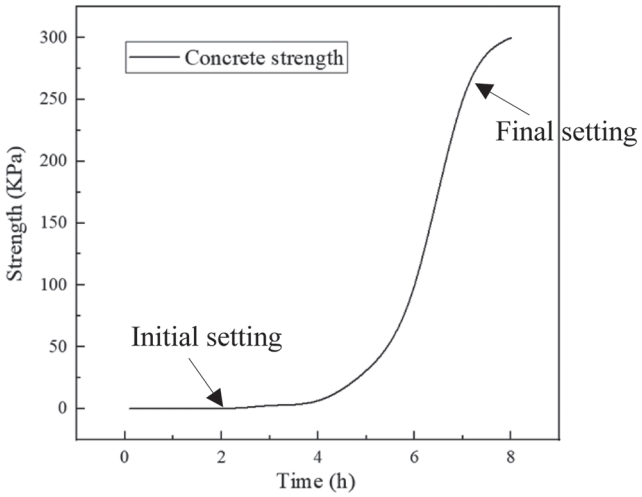

FIGURE 4 Relationship between time and concrete strength[11]

TABLE 1 Parameters of the cement paste

Parameters	K_{cw}	K_{fw}	K_{solid}	K_{air}	α
Values	4	82	4	1	0.5

$$f_1+f_2+f_3+f_4=1 \tag{5}$$

where K is the calculated dielectric constant of the mixed material. f_1, f_2, f_3, f_4, and K_{fw}, K_{cw}, K_{solid}, and K_{air} are the volume fractions and the dielectric constants of free water and gel water, bond water, cement gel and air, respectively. α is an exponential index with an empirical value of 0.5 for all the dielectric constants.[58] The parameters used in Equation 4 are listed in Table 1.

As the dielectric constant of free water is significantly larger than that of bond water, cement gel, and air, the combined dielectric constant of cement paste is governed by the amount of free water. To simplify the calculation and highlight the effect of free water, the cement paste is divided into free water and other components in the practical calculation; thus, Equation 4 can be rewritten as

$$K^{\alpha}=f_1K_{fw}^{\alpha}+f_5K_{other}^{\alpha} \tag{6}$$

$$f_1+f_5=1 \tag{7}$$

where K_{other}^{α} and f_5 are the dielectric constant and volume fraction of other components.

Since the effects caused by other components are negligible, the dielectric constant of cement paste could be expressed as a function of the free water content by Equation 6, which is illustrated in Figure 5. The dielectric constant with a unit of 1 is relative permittivity, which is defined as the specific value of the capacitance of a capacitor filled with the given material to the capacitance of an identical capacitor in a vacuum without any dielectric material. From Figure 5, the dielectric constant of cement paste varies linearly with the free water content. Therefore, the dielectric constant can be utilized to show the change of free water content.

2.4 | Effect of the covering dielectric material

When the monolithic patch antenna is covered by certain dielectric or covering materials, their effect on the resonant frequencies of the underlying patch antenna needs to be investigated. To reduce computation complexity, a simplified

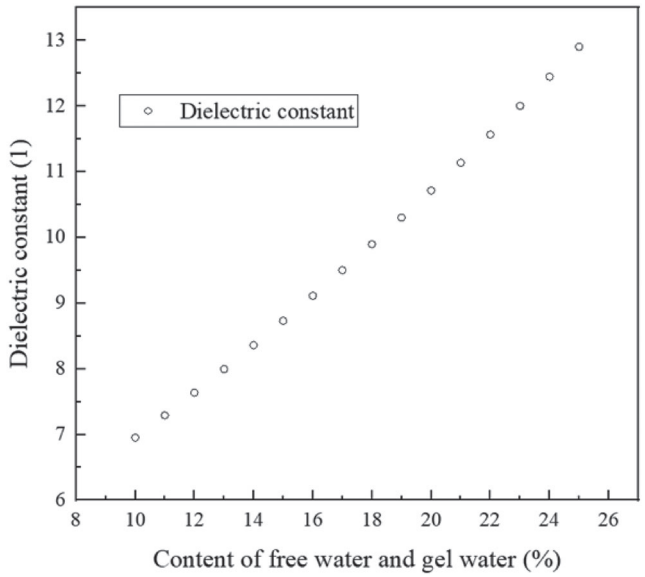

FIGURE 5 Relationship between free water change and dielectric constant of cement paste

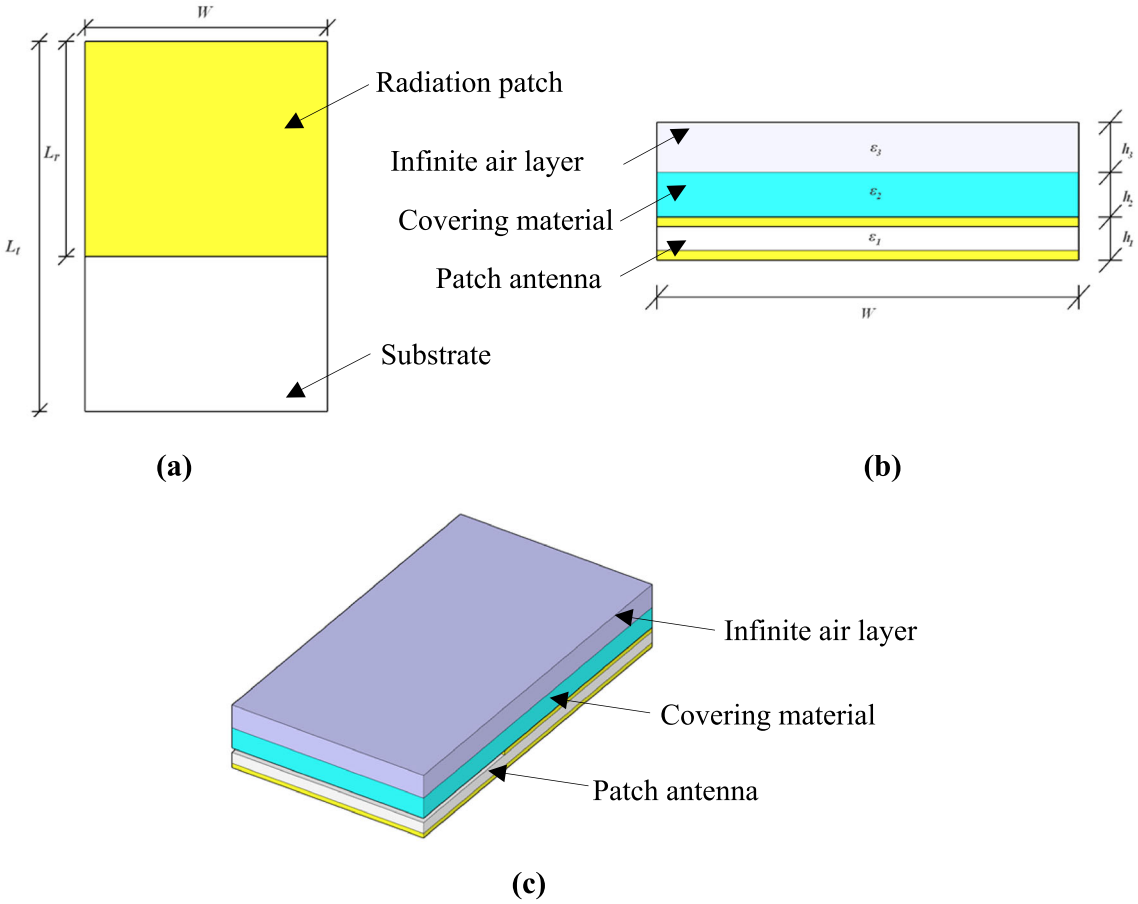

FIGURE 6 Schematic diagram for the covered rectangular patch antenna sensor (a) top view, (b) front view, and (c) axonometric drawing

physical model is proposed in Figure 6, with an infinite air layer (gray area) and a covering material layer (blue area) in direct contact with the radiation patch. The electric flux originating from the radiation patch is deflected when passing through the interface between two different covering dielectric layers,[26–29] and the resonant frequencies of the covered

patch antenna change with the dielectric constant variation of the covering materials. According to the theory of conformal mapping and the concept of equivalent capacitance, the effect induced by the covering material can be analyzed by introducing an equivalent model of an uncovered patch antenna replacing the original multilayer model,[27,29] as depicted in Figure 7, where W is the width of the monolithic patch antenna, L_r is the length of the radiation patch, L_t and is the length of patch antenna; thus, ε_1, ε_2, and ε_3 are the dielectric constants of the patch antenna, covering material and infinite air layer, respectively. h_1, h_2, and h_3 are the heights of the patch antenna, covering material, and infinite air layer, respectively.

Assuming that the height of the top air layer h_3 is infinite compared to h_1 and h_2, the electric flux path, originating from the radiation patch, has three modes, A, B, and C, as shown in Figure 7a. Path A refers to the electric flux crossing the dielectric board directly. Path B refers to the electric flux going through the covering material and dielectric board, and Path C refers to the electric flux passing through the infinite air, covering material, and dielectric board. Considering the capacitive contribution of each electric flux path, Path A could be equivalent to region S_1; Path B could be equivalent to region S_2 and to parts of S_4 and S_5. Path C could be equivalent to region S_3 and parts of S_4 and S_5.

The antenna width will be enlarged due to the nonlinear flux path. The effective width W_{ef} of the equivalent patch antenna can be calculated as[29]:

$$W_{ef} = W + \frac{2 \times h_1}{\pi} \times \ln\left[17.08\left(\frac{w}{2 \times h_1} + 0.92\right)\right] \tag{8}$$

Then the filling fractions q_1, q_2, and q_3 representing the capacitive effect of three regions with different dielectric constants are expressed by Equations 9–11[29]:

$$q_1 = 1 - \frac{h_1}{2W_{ef}} \ln\left(\frac{\pi}{h_1} \times W_{ef} - 1\right) \tag{9}$$

$$q_2 = 1 - q_1 - \frac{h_1 - v_\varepsilon}{2W_{ef}} \ln\left[\left(\frac{\pi}{h_1} \times W_{ef} \frac{\cos\left(\frac{\pi v_\varepsilon}{2h_1}\right)}{\pi\left(\frac{h_2}{h_1} - \frac{1}{2}\right) + \frac{\pi v_\varepsilon}{2h_1}} + \sin\left(\frac{\pi v_\varepsilon}{2h_1}\right)\right)\right] \tag{10}$$

$$q_3 = \frac{h_1 - v_\varepsilon}{2W_{ef}} \times \ln\left[\left(\frac{\pi}{h_1} \times W_{ef} \frac{\cos\left(\frac{\pi v_\varepsilon}{2h_1}\right)}{\pi\left(\frac{h_2}{h_1} - \frac{1}{2}\right) + \frac{\pi v_\varepsilon}{2h_1}} + \sin\left(\frac{\pi v_\varepsilon}{2h_1}\right)\right)\right] \tag{11}$$

where the quantity v_ε is given by Equation 12 as

$$v_\varepsilon = \frac{2h_1}{\pi} \arctan\left[\frac{\pi}{\frac{\pi \times W_{ef}}{2h_1} - 2}\left(\frac{h_2}{h_1} - 1\right)\right] \tag{12}$$

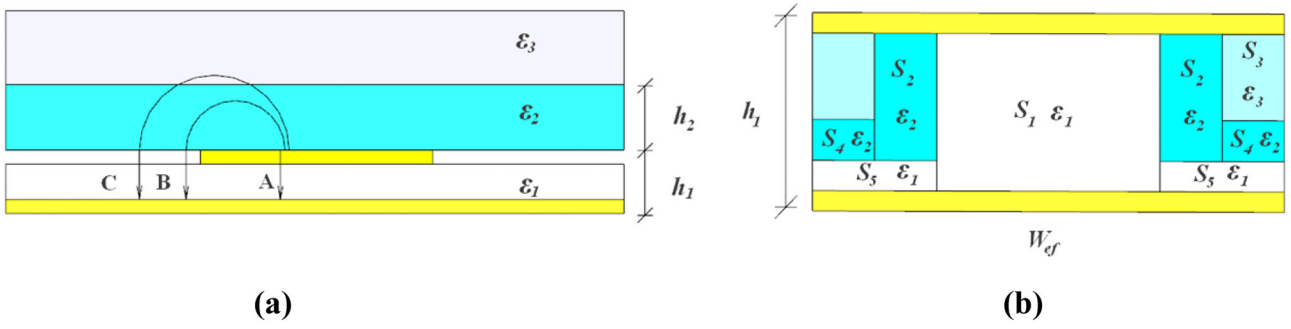

FIGURE 7 Schematic diagram for (a) the equivalent schematic diagram of the magnetic induction line and (b) the equivalent model[27]

Because the filling fraction expressions in the ultimate limit state are ignored when there is no covering material, Equations 8–12 overestimate the effect of the second layer dielectric board with a dielectric constant of ε_2. To rectify the error, a new filling fraction q_4 is proposed by Equation 13[27]:

$$q_4 = \frac{h_1}{2W_{ef}} \times \ln\left(\frac{\pi}{2} + \frac{h_1}{2W_{ef}}\right) \tag{13}$$

The two filling fractions q_1 and q_2 are then modified as q_{1n} and q_{2n} by Equations 14 and 15:

$$q_{1n} = q_1 - q_4 \tag{14}$$

$$q_{2n} = 1 - q_{1n} - q_3 - 2q_4 \tag{15}$$

The effective dielectric constant ε_e of the covered antenna can be calculated by

$$\varepsilon_e = \varepsilon_1 q_{1n} + \frac{\varepsilon_1(1-q_{1n})^2 \times \left[\varepsilon_2^2 q_{2n} q_3 + \varepsilon_2 \varepsilon_3 \left(q_{2n} q_4 + (q_3+q_4)^2\right)\right]}{\varepsilon_2^2 q_{2n} q_3 q_4 + \varepsilon_1(\varepsilon_2 q_3 + \varepsilon_3 q_4)(1-q_{1n}-q_4)^2 + \varepsilon_2 \varepsilon_3 q_4 \left[q_{2n} q_4 + (q_3+q_4)^2\right]} \tag{16}$$

Considering the effect of the effective length extension, the adjusted effective dielectric constant $\varepsilon_e^{'}$ is rewritten as

$$\varepsilon_e^{'} = \frac{2\varepsilon_e - 1 + K}{1+K} \tag{17}$$

where K is:

$$K = \sqrt{\frac{W_{ef}}{W_{ef} + 10h_1}} \tag{18}$$

Finally, the resonant frequencies f of the equivalent patch antenna are obtained by Equation 19:

$$f = \frac{cn}{2L_r\sqrt{\varepsilon_e^{'}}} \tag{19}$$

where c is the speed of light, and n is the order of resonant frequency.

The resonant frequencies of the covered patch antenna are only related to the dielectric constant and the height of the covering material when the patch antenna is buried inside the fresh cement paste. Due to the low gain of the higher order of resonant frequencies, the fundamental resonant frequency f_1 is selected as the sensing parameter and defined in Equation 20.

$$f_1 = \frac{c}{2L_r\sqrt{\varepsilon_e^{'}}} \tag{20}$$

3 | NUMERICAL SIMULATION

To investigate the relationship between the moisture content and fundamental resonant frequency, this section presents the simulation using the estimation equations in Section 2 and the Ansoft high-frequency structure simulator (HFSS).

3.1 | Simulation by equivalent model

Based on Equations 20 and 22, a normal patch antenna functioning at around 2.45 GHz is designed, and the parameters of the patch antenna are listed in Table 2. Assuming the patch antenna is placed inside fresh cement paste, the material of the top layer is set as air and the material of the second layer is set as cement paste according to the model. The height of the air is infinite to simulate the outer space.

$$W \leq \frac{c}{2f_{be}}\sqrt{\frac{\varepsilon_e+1}{2}} \tag{21}$$

$$L_r = \frac{c}{2f\sqrt{\varepsilon_e}} \tag{22}$$

The relationship between the dielectric constant of covering material ε_2 and fundamental resonant frequency is investigated by Equation 19 and is illustrated in Figure 8. From the data in Sections 2.2 and 2.3, the moisture content changes from 22% to 16% during the early-age hydration period, causing the dielectric constant of the covering material ε_2 to shift from 12 to 8. To simulate the hydration process reasonably, the height of the second layer dielectric constant h_2 is set at 20 mm and the dielectric constant of covering material ε_2 changes from 5 to 13 in this calculation example.

Figure 8 presents a nearly linear relationship between the shift of fundamental resonant frequency and dielectric constant ε_2. The fundamental resonant frequency decreases from 2.36 to 2.32 GHz with about 40 MHz difference when the dielectric constant varies from 8 to 12. This is consistent with the results[44] presented in Section 2.1. In general, the temperature effect can be ignored in the sensor design.

When a normal patch antenna is embedded inside a high-loss material, the gain of the patch antenna sensor will decrease and further degrade the far-field communication capability. In general, when the covering material is determined, the far-field communication capability of the embedded antenna sensor will be compromised by the increased

TABLE 2 Setting domain for parameters of the patch antenna

Parameters	W (mm)	L_r (mm)	L (mm)	f (GHz)	ε_1	h_1 (mm)
Dimensions	51	41.3	54.3	2.45	2.2	0.508

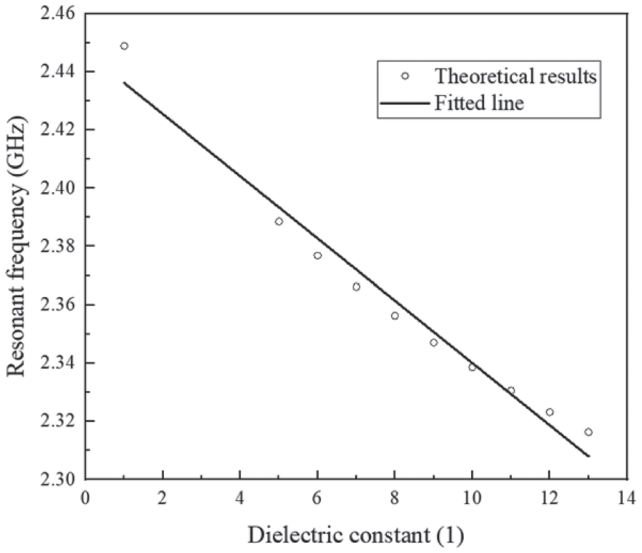

FIGURE 8 The relationship between the dielectric constant of the covering material and fundamental resonant frequency of the covered patch antenna

height of the covering-material. However, the fundamental resonant frequency is also influenced by the height of the covering material due to the reconstitution of the near-field magnetic distribution. Hence, it is necessary to find an appropriate height range to satisfy the far-field communication demand while keeping the fundamental resonant frequency independent (i.e., out of range) for an uncorrelated relationship with the covering height.

The effect of the covering material height is considered in Equation 20 and shown in Figure 9. In this calculation example, the dielectric constant ε_2 is set as 10, and the height of the second layer varies from 0 to 40 mm.

In Figure 9, the fundamental resonant frequency of the covered patch antenna drops significantly when the cement paste starts to cover the patch. But the pace of frequency decline slows down with the increasing height of the covering material, and keeps almost constant after the cement height reaches 35 mm. The covering-material's height must be over 25 mm to eliminate the effects induced by near-field reconstitution. The thicker the cement paste is that covers the patch, the weaker the far-field communication capability becomes. According to Zhou's survey,[49] the far-field communication distance decreased to 0.11 m when the height reached 80 mm. To minimize the influence brought by the covering height and guarantee the far-field communication capability, it is suggested that the covering height should be in the range of 25 to 80 mm. Besides, the far-field communication distance will be affected by the antenna design, so it is necessary to further confirm the height range by the simulation based on a specific design, which is described in Section 3.2.

3.2 | Simulation in HFSS

The effects of the dielectric constant shift and height change are analyzed using the Ansoft high frequency structure simulator (HFSS). The basic HFSS model consists of a covered patch antenna and a covering material with a changeable height and dielectric constant, which is shown in Figure 10. The covered patch antenna is fed by a wave port at the end of the antenna. The model is fully surrounded by an air container. The maximum size of the air container is about a quarter wavelength to ensure computational accuracy of the far field radiation. The radiation patch and ground plane are set as Perfect Electric (Perfect E) to satisfy the property of metal, and the material of the dielectric substrate is set as RT/Duroid 5880. All the parameters of the patch antenna duplicate the parameters in Table 1.

Like the calculation example in Section 2.4, the dielectric constant of the covering material is changed from 5 to 13 in simulation. For each dielectric constant step, the return loss curve is acquired and shown in Figure 11a. The fundamental resonant frequency of each step is then extracted from the lowest point of the return loss curve, plotted in Figure 11b.

From Figure 11b, the fundamental resonant frequency of the patch decreases with the increase of the dielectric constant both for simulation and theoretical results, except a step increase at the middle. This step increase is mainly caused by the influence of a higher order frequency happened when the dielectric constant of the covered material

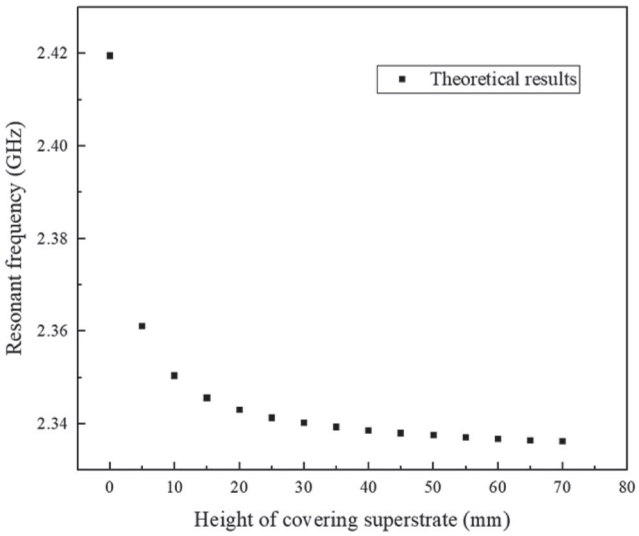

FIGURE 9 Relationship between the height of the covering material and the fundamental resonant frequency of the covered patch antenna

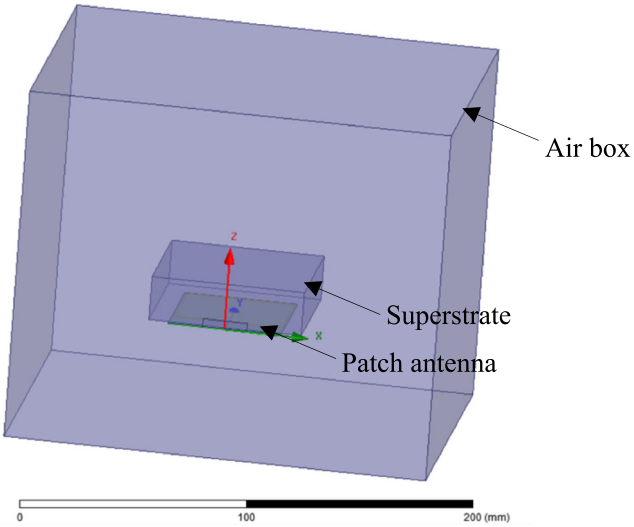

FIGURE 10 Simulation model of Ansoft high frequency structure simulator (HFSS)

increased to 7, as shown in Figure 11a. Assuming dielectric constant equal to 10, the current distribution at 2.26 and 2.8 GHz is then analyzed. From the current distribution, it is obvious that a higher order is caused. However, since only the trend is analyzed to get the setting time, the step increase can be ignored to simplify the analyzation. The decrease shift caused by the variation of moisture content and the slope of the two fitted lines shown in Figure 11b are almost equivalent, which means that the fundamental resonant frequency decreases caused by the covering material (about 40 MHz) is much higher than the temperature effect (about 2 MHz) during the cement hydration.

The relationship between the height of the covering material and fundamental resonant frequency of the rectangular patch is then simulated with the same parameters as in Section 2.3. The dielectric constant ε_2 is set at 10 and the height of the second layer varies from 5 to 40 mm with each step of 5 mm. The return loss curve and fundamental resonant frequency are shown in Figure 12.

With the increase of the covering-material's height, both the simulated and theoretical results changed rapidly at first (before 15 mm) and then started to converge to a constant (after 25 mm). Compared with theoretical results, while the shift of fundamental resonant frequency in simulated results has more fluctuation with a covering height of less than 15 mm, the frequency variation seemed to stabilize when the height was over 20 mm. In order to minimize the influence induced by the covering height and concentrate on the effect of the dielectric shift, the height of the covering material should be greater than 25 mm for practical use. Furthermore, the return loss of the patch antenna is higher than -8 dB when the height of the covering material achieves 35 mm. Combining the results from the equivalent model and HFSS simulation for the used patch antenna sensor, the covering height should be higher than 25 mm and less than 40 mm.

4 | EXPERIMENT

The experiments are designed to test the performance in the setting time prediction of the proposed patch antenna sensor. The patch antennas for experiments are fabricated using RT/Duroid 5880 and copper, which are the same material used in the simulation model in Section 3. In addition, P. I 42.5 Portland cement without any admixture was chosen for the experiment.

4.1 | Setting time experiment

4.1.1 | Testing methods for experiments

For the patch antenna sensor, the fundamental resonant frequency was wired measured by a vector network analyzer (VNA) every 10 min. In the future analyzation, it can be interrogated wirelessly by adding RFID chip[59] or using a

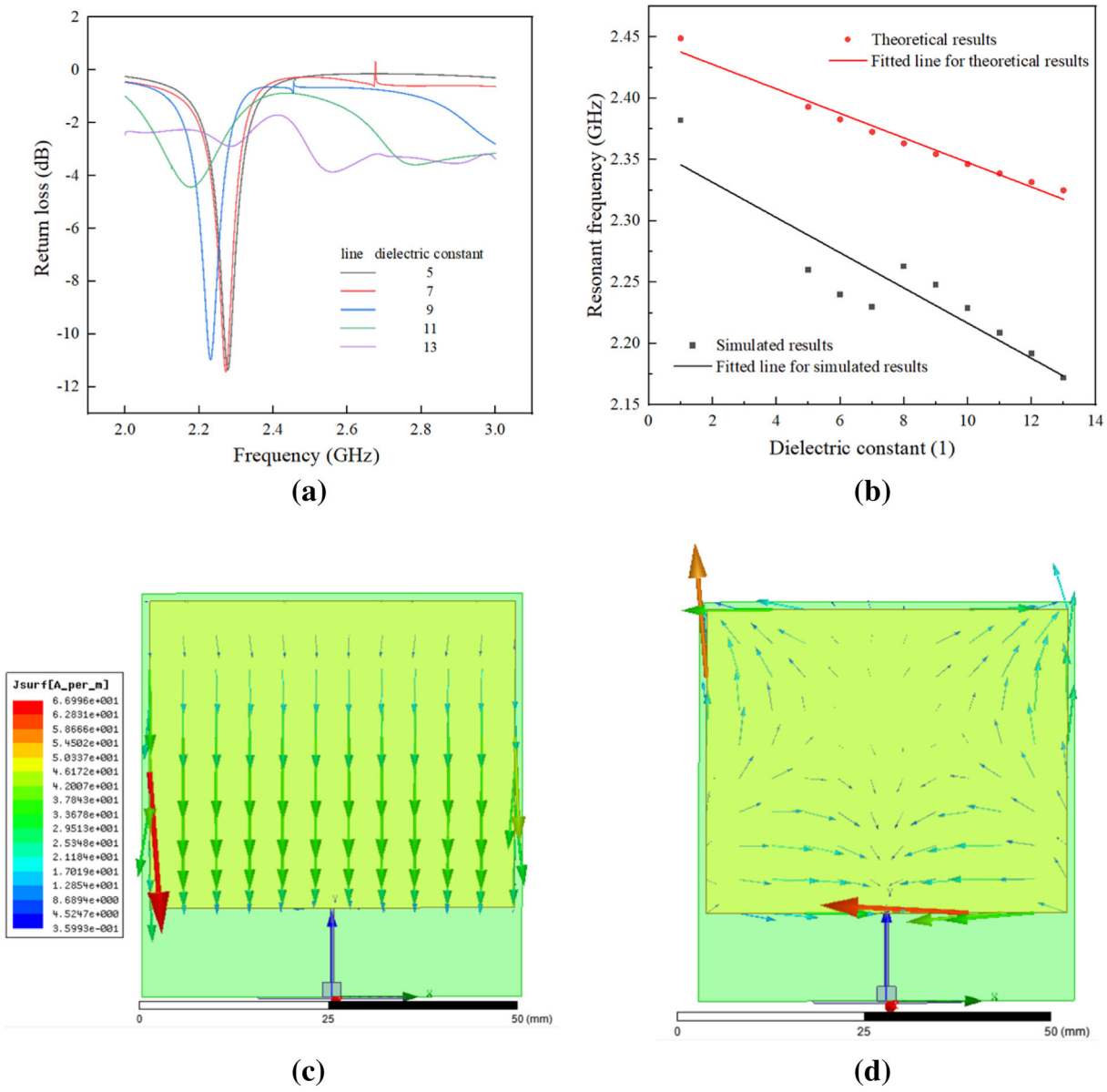

FIGURE 11 Relationship between dielectric constant of covering material and fundamental resonant frequency. (a) Return loss curve, (b) scatter diagram for simulated and theoretical results, (c) current distribution at 2.26 GHz, and (d) current distribution at 2.8 GHz

FMCW radar directly.[43] To ensure testing accuracy, each test was repeated three times. The performance of the antenna sensor was evaluated by comparing the measured setting time with the results of Vicat test.

A Vicat apparatus was used to test the penetration depth of the cement. The cement from the same batch was placed in a container and a thin testing needle was injected into the cement every 30 min until the depth of penetration was lower than 70 mm. After that, the test was repeated every 5 min and when the penetration depth reached 65 mm, that depth was regarded as the initial setting depth of cement.[60] Then the container was turned over, and the bottom surface of the paste with a better flatness was tested by a thicker needle. The final setting happened when the striker could not leave scars on the surface of the cement paste.

4.1.2 | Instrumentation setup

Figure 13 shows the experimental setup. Three containers made of acrylic acid held the Portland cement paste covering an antenna sensor at the bottom of the cement paste. The patch antenna inside the container is wrapped by laminating

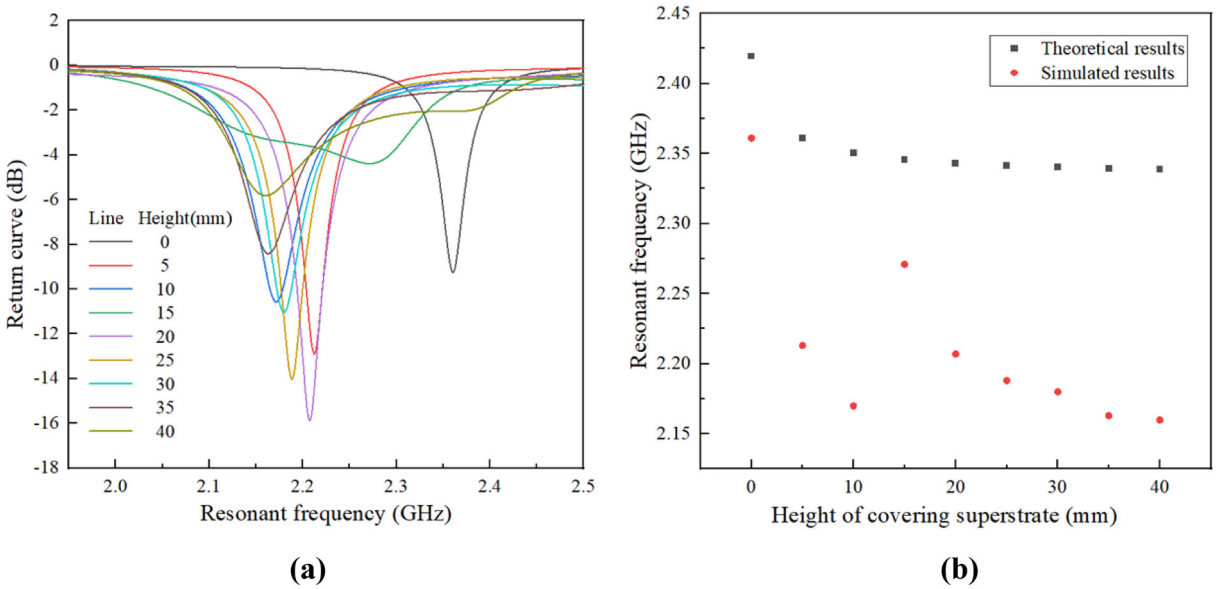

FIGURE 12 The relationship between the height of the covering material and the fundamental resonant frequency. (a) The return loss curve and (b) the scatter diagram for simulated and theoretical results

film to prevent the radiation patch of the antenna from contacting the free water directly. A small hole was drilled through the sidewall of container to hold a VNA connector. About 1500-g cement paste was mixed and then filled up three acrylic acid containers and an additional container for the Vicat test. These containers were then air cured while tested by the VNA and Vicat apparatus until the final setting of the paste.

4.1.3 | Group arrangement

Three groups with varying parameters were tested and are listed in Table 3. The container for each group was the same size. Group 1 was set as the reference set. As shown in Figure 14, an acrylic waterproof sheet was placed above the patch antenna in Group 2 to investigate the effect of the encapsulating material. The height of cement paste was set at 60% of the reference set to test the measurement accuracy when there was a difference between the buried depth.

The mix proportion of the testing cement was determined by the setting time measurement standard GBT1346-2011[60] and listed in Table 4. To ensure the accuracy of the test, the mix proportion kept constant during the full process of the experiment.

4.1.4 | Results and discussion

The Vicat setting time as measured by the Vicat apparatus was selected as the comparison value and displayed in Part A. Then the fundamental resonant frequencies measured from three patch antenna sensors were used to calculate the setting time of the cement paste and then compared with the value measured by Vicat apparatus, which is shown in Part B.

Vicat apparatus test

The Vicat needle's depth of penetration into the cement as a function of time is shown in Figure 15. Since the initial setting happens when the depth of penetration decreased from 67 to 65 mm[54] it was seen to occur at 215 min for the cement paste.

The distinct degree of the scar caused by the needle is shown in Table 5. The final setting time was determined as 310 min for the scar, which could not be recognized.

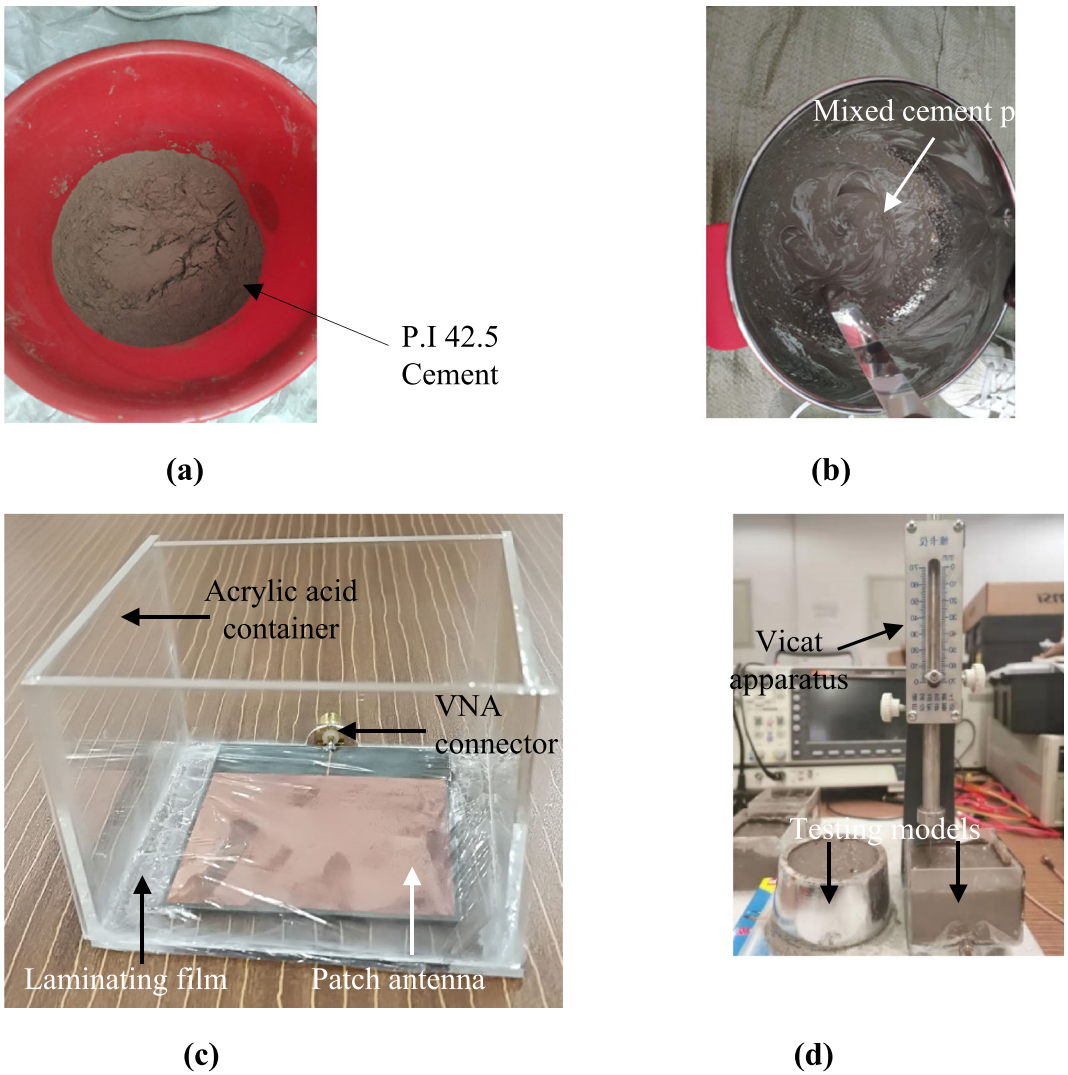

FIGURE 13 Experimental setup. (a) Portland cement, (b) the cement paste mixture, (c) the fabricated patch antenna, and (d) the Vicat test apparatus

TABLE 3 Parameters for the three experiment groups

Parameter	Group 1	Group 2	Group 3
Maximum height of cement paste (mm)	50	50	30
Height of container (mm)	52		
Length of container (mm)	73		
Width of container (mm)	66		
Adding waterproof sheet	No	Yes	No

Measuring for setting time using patch antenna

At the beginning of the experiment, the influence of cement height in the experiment was analyzed and compared with the simulated and theoretical results in Section 3. The relationship between the height of cement paste and the fundamental resonant frequency of the covered patch antenna is shown in Figure 16.

The fundamental resonant frequency in the experiment varied greatly with the height—less than 10 mm—but keeps nearly constant when the covering height is larger than 15 mm, which is duplicated in the simulation.

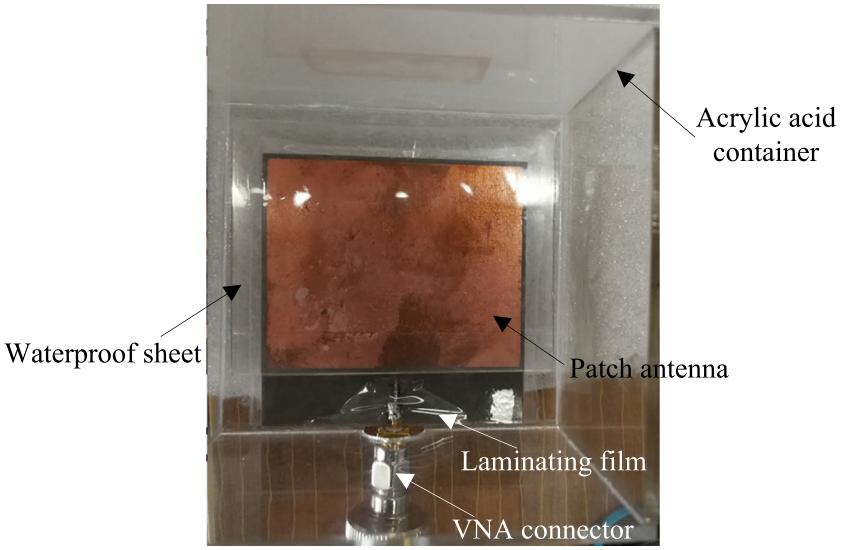

FIGURE 14 Top view of the acrylic acid container in Group 2

TABLE 4 Mix proportion of cement net slurry

Ingredient	Portland cement	Water
Mix proportion (%)	77.2	22.8

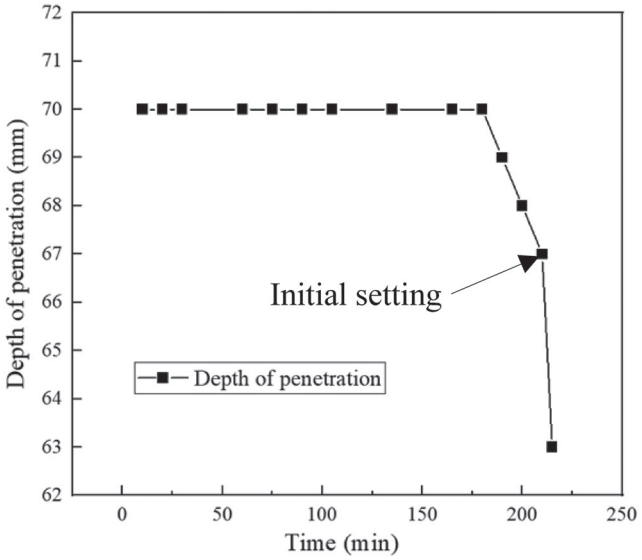

FIGURE 15 Relationship between time and depth of penetration

TABLE 5 Distinct degree designation based on visual identification of the crack scar

Time	230	260	290	295	300	310	315	320
Degree	Clear	Clear	Only half	Only half	Only half	Unable to recognize	Unable to recognize	Unable to recognize

The measured fundamental resonant frequencies of these groups are shown in Figure 16. As the dielectric constant of the covering dielectric board in Group 2 is lower than the dielectric constant of the dielectric board, the fundamental resonant frequency of Group 2 will increase compared to Group 1 without the covering board. The difference between

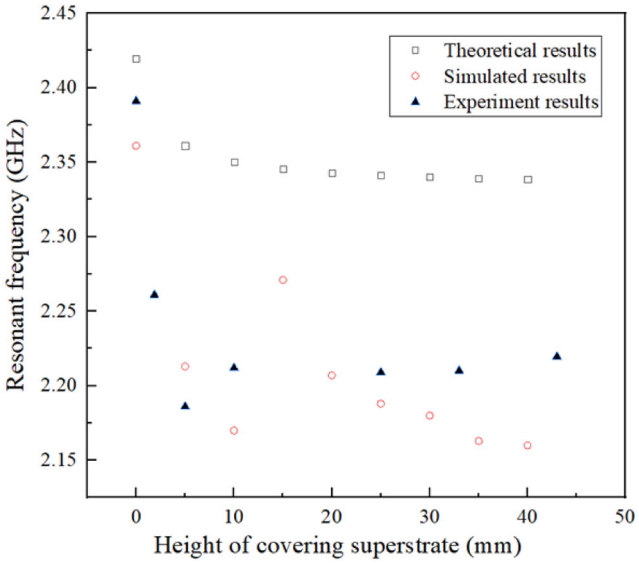

FIGURE 16 Relationship between height of covering material and fundamental resonant frequency

the theoretical calculation, simulation, and experiment results mainly comes from the different boundary conditions among each other. Actually, there is a laminating film under the patch antenna. This film is estimated by adding an air gap in simulation and totally ignored in theoretical calculation. Besides, the covering cement paste is regarded as a uniform dielectric in the simulation. These differences may cause several differences in the final results, but the change trend of the results is similar. The fundamental resonant frequency of Group 1 is similar to that of Group 3, indicating that the height of cement paste has little influence on the fundamental resonant frequency of the covered patch antenna when the covering height is high enough (e.g., more than 30 mm in this experiment).

For all three groups, the fundamental resonant frequencies started lower and then increased rapidly along with the hydration process. Finally, the fundamental resonant frequencies of the three groups converged to a level. The pattern of the frequency change curves is like an inverted-Z, which is similar to the change tendency of moisture content shown in Figure 3. That is, the setting state can be predicted by analyzing the change rate of the measured resonant frequencies.

Based on the results in Section 3, the initial setting time could be directly regarded as the time when the fundamental resonant frequency (moisture content) starts to increase rapidly. The initial setting time was obtained from Figure 17, which is 255 min for Group 1, 175 min for Group 2, and 250 min for Group 3.

During the test, the amount of moisture content was sampled at regular intervals. The relationship between moisture content and time appears as a set of scattering data. To calculate the differential coefficient at time t (point n), a moving window from point $n - m$ to point $n + m$ is established. Then, the $2m + 1$ continuous scatters were used for linear fitting, and the slope of the fitted line is regarded as the differential coefficient of point n at time t in the moving window.

The change rate was then used to evaluate the final setting time quantitatively. A moving window contained nine continuous scatters (can also be referred to as 5, 7 or 11 scatters since the results are similar), which were used for liner fitting, and the slope of the fitted line is regarded as the change rate of point n in the moving widow. Based on Equation 2, the final setting time is regarded as the time when the change rate starts to decrease from the maximum data.

The relationship between time and change rate is shown in Figure 18. The final setting time was then obtained from this Figure, which is 320 min for Group 1, 285 min for Group 2, and 310 min for Group 3.

The setting time measured by the Vicat apparatus and the patch antenna sensor is compared in Table 6. The table also shows the average error for each group.

Although the height of cement paste and coverings were different between the three groups, the calculated three initial setting times and final setting time are similar to the results obtained from the Vicat apparatus. That is, the setting time sensing is mostly dependent on the change tendency of the resonant frequency and less affected by the

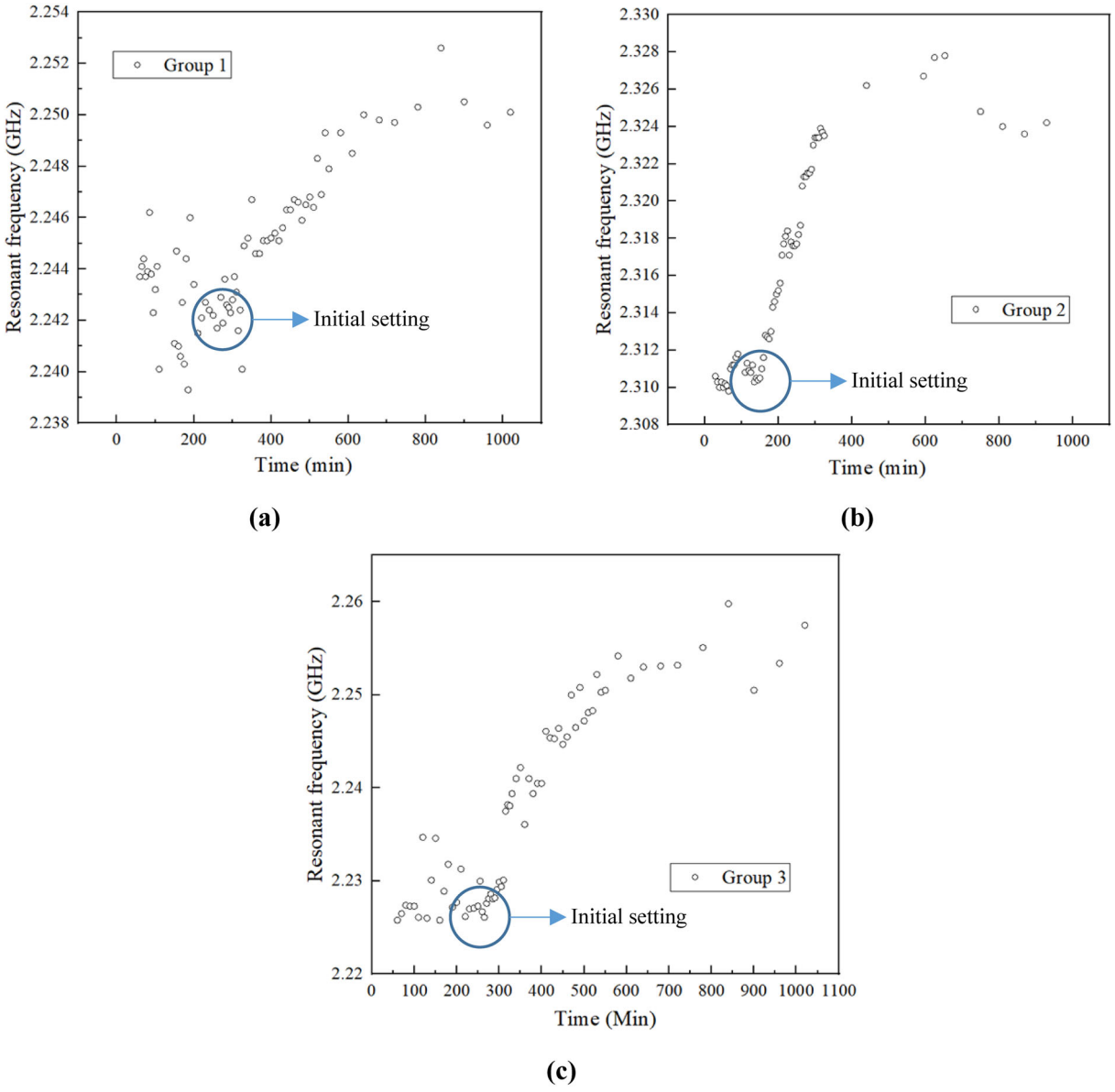

FIGURE 17 Relationship between time and fundamental resonant frequency in (a) Group 1, (b) Group 2, and (c) Group 3

dielectric load or environment noise. The error for the initial setting time and final setting time was below 20% and 10%, respectively, and the average error for the three groups was below 6%. This exhibits a great workability in setting time sensing.

4.2 | Moisture content detection after hardening

4.2.1 | Testing methods for experiments

After the setting time experiment, another test was arranged to verify the application of moisture content detection after cement hardening, which mainly relates to the sensitivity of the patch antenna to the surrounding water.[61] Figure 4 shows the experimental setup. Additional water was injected into the specimen by a dropper. The amount of injected water was controlled by an electronic scale shown in Figure 4b, and the resonant frequency of the patch antenna sensor was determined by the VNA, which was the same VNA used in Section 4.1.

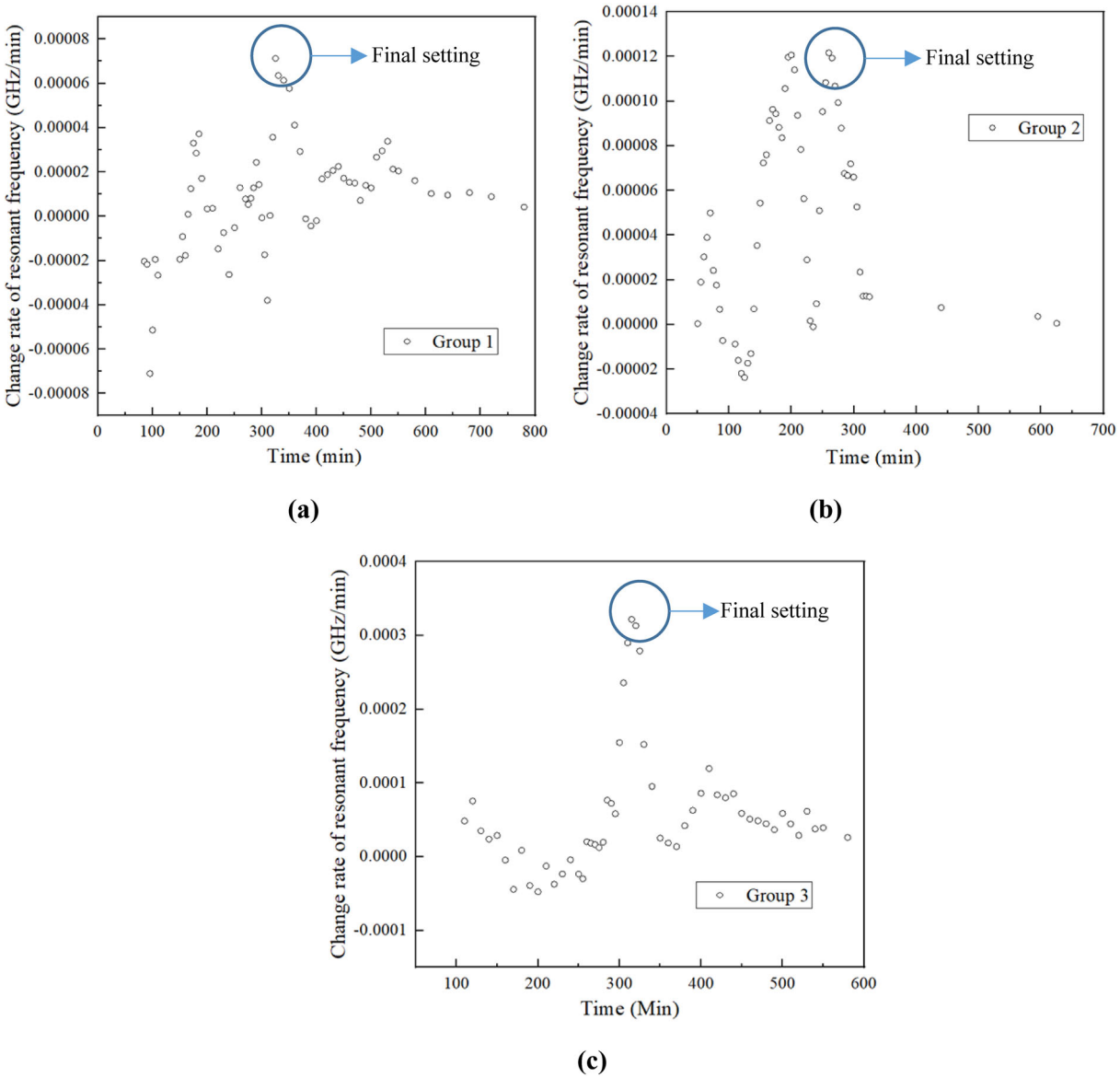

FIGURE 18 Relationship between time and change rate of fundamental resonant frequency (a) Group 1, (b) Group 2, and (c) Group 3

4.2.2 | Instrumentation setup

As shown in Figure 19, the specimens used in setting time sensing after hardening were utilized for moisture content detection in this experiment. After finishing the setting time measurements, some cracks were randomly made by sticking a knife in and out the cement pastes to simulate crack openings. After air cured for 15 days, a small amount of water was injected into three cement pastes along their cracks with an increment of 0.5 ml. Two minutes after each injection, the fundamental resonant frequency of each embedded patch antenna was measured three times in 1 min. The tested resonant frequencies were used to show the amount of injected water presented in Section 4.2.3.

4.2.3 | Results and discussion

The relationship between fundamental resonant frequency of the embedded patch antenna and quantity of injected water is shown in Figure 20.

TABLE 6 Comparison of three experiment groups obtained by Vicat

Parameters	Vicat	Group 1	Group 2	Group 3	Average	Error (%)
Initial setting time (min)	215	255	175	250	203.3	5.4
Error (%)	/	18.6	18.6	16.3		/
Final setting time (min)	310	320	285	310	305	1.6
Error (%)	/	3.2	8.1	0		/

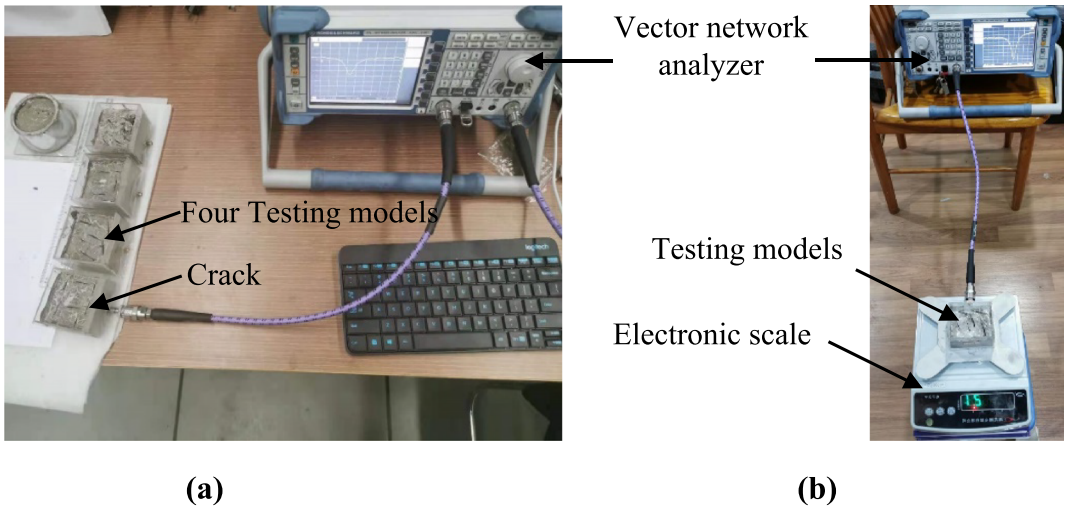

FIGURE 19 Experiment setup (a) VNA testing and (b) experiment testing of moisture content detection

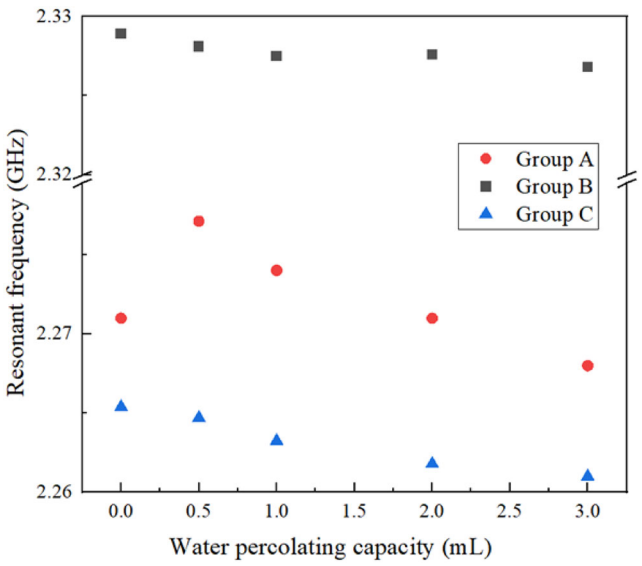

FIGURE 20 Relationship between moisture content and fundamental resonant frequency after hardening

When the water penetrates the cement paste, the dielectric constant of cement paste will increase and further decrease the fundamental resonant frequency of the covered patch antenna sensor according to the theory of magnetic flux, which is consistent with the experiment results shown in Figure 18. A nearly linear relationship is shown in all three groups. Since the produced cracks were randomly created, the water inside the cracks was considered to be uniformly distributed in the cement. The cement volumes of Groups 1, 2, and 3 were 240.9, 144.5, 240.9 cm^3, respectively;

thus, the minimum resolution in the moisture content rate of the three groups was 2.07%, 3.46%, and 2.07% respectively. Hence, the antenna sensor can be used to monitor the small moisture content change of cement after hardening. Since the antenna sensor is designed to be embedded into the structure, it can be utilized as a leakage detection sensor during the service stage. However, the sensitivity of the injected water is about 2 MHz/ml, which is similar to the frequency shift caused by temperature change. That is, the moisture content prediction is easily affected by temperature variation. Furthermore, the fundamental resonant frequency will continually shift for a short time after each injection, which signifies that the patch antenna sensor is only sensitive to adjacent injected water. Furthermore, remote water is difficult to detect due to limited sensitivity. In general, to effectively use the patch antenna sensor in practice, temperature calibration and a redesign focusing on sensitivity improvement is necessary.

5 | CONCLUSION AND COMMENTS

This paper introduced a passive patch antenna sensor for measuring the setting time of cement and moisture content detection after hardening. The fundamental resonant frequency shift of an embedded patch antenna can be utilized to define sensing parameters for the moisture content in cement paste. An equivalent model based on the magnetic flux theory and simulated model in HFSS was adopted to verify design availability. Then, the resonant frequency shift caused by the change of dielectric constant and temperature effect were compared in a theory model, in the simulation, and in the experiment. The temperature effect was about 10 times lower than the change caused by the dielectric constant shift, which indicated that the temperature effect could be ignored in future experiments setting time sensing values.

Two experiments were carried out to detect the cement setting time before hardening and the moisture content change after hardening. A moving window was utilized to calculate the change rate of the fundamental resonant frequency shift. The initial setting time was obtained from the change tendency of the fundamental resonant frequency shift, and the final setting time was determined based on the time when the change rate started to decrease from the maximum value to an average error lower than 6%. Since the measured setting time only related to the change rate of the fundamental resonant frequency, it was less affected by the environmental noise and the random material distribution inside the concrete. Furthermore, the moisture content detection experiment showed that the embedded patch antenna sensor was highly sensitive to the injected water with a moisture rate of more than 3.46%. The two experiments indicate that an antenna sensor can be utilized for detecting setting time during cement hydration and for predicting leakage in the service time. Future research includes the development of temperature calibration, decouple or minimization of temperature effect, and a redesign for sensitivity improvement to improve workability after cement hardening.

ACKNOWLEDGMENTS

This research was funded by the National Natural Science Foundation of China (grant no. 52078375, 52178298), the Key Laboratory of Performance Evolution and Control for Engineering Structures (Tongji University), the Ministry of Education of the People's Republic of China (grant no. 2018KF-4).

ORCID

Zhuoran Yi https://orcid.org/0000-0002-4204-2079
Liyu Xie https://orcid.org/0000-0001-5777-0645

REFERENCES

1. Budoya DE, Baptista FG. A comparative study of impedance measurement techniques for structural health monitoring applications. *IEEE Trans Instrum Meas*. 2018;67(4):912-924.
2. Cawley P. Structural health monitoring: closing the gap between research and industrial deployment. *Struct Health Monit*. 2018;17(5):1225-1244.
3. Weihnacht B, Lieske U, Gaul T, Tschöke K *Structural Health Monitoring*. 2018.
4. Brooks JJ, Johari MM, Mazloom M. Effect of admixtures on the setting times of high-strength concrete. *Cem Concr Compos*. 2000;22(4):293-301.
5. Demir I, Sevim O, Tekin E. The effects of shrinkage-reducing admixtures used in self-compacting concrete on its strength and durability. *Constr Build Mater*. 2018;172:153-165.

6. Spencer BF Jr, Ruiz-Sandoval ME, Kurata N. Smart sensing technology: opportunities and challenges. *Struct Control Health Monit*. 2004; 11(4):349-368.
7. Han F, Zhang Z. Hydration, mechanical properties and durability of high-strength concrete under different curing conditions. *J Therm Anal Calorim*. 2018;132(2):823-834.
8. Persson B. Hydration and strength of high performance concrete. *Adv Cem Based Mater*. 1996;3(3-4):107-123.
9. Loukili A, Khelidj A, Richard P. Hydration kinetics, change of relative humidity, and autogenous shrinkage of ultra-high-strength concrete. *Cem Concr Res*. 1999;29(4):577-584.
10. Pane I, Hansen W. Concrete hydration and mechanical properties under nonisothermal conditions. *ACI Mater J*. 2002;99(6):534-542.
11. Lootens D, Bentz DP. On the relation of setting and early-age strength development to porosity and hydration in cement-based materials. *Cem Concr Compos*. 2016;68:9-14.
12. British Build Code, British Standard for the Design and Construction of Reinforced and Prestressed Concrete Structures, BS 8110.
13. Technical Committee CEN/TC 51. "Cement and building limes" European building code, Products and systems for the protection and repair of concrete structures - Test methods - Determination of watertightness of injected cracks without movement in concrete, prEN 14068-2003.
14. Akram KJ, Islam T, Ahmed A. A simple method on transformer principle for early age hydration monitoring and setting time determination of concrete materials. *IEEE Sensors J*. 2018;18(17):7265-7272.
15. Technical Committee CEN/TC 51. "Cement and building limes" European building code, methods of testing cement—Part 3: Determination of setting times and soundness, EN 196-3-2016.
16. Ham Y, Kim Y, Koo M, Kim S, Lee BYK. Analysis on behavior of adiabatic temperature rise of concrete considering final setting time. *J Archit Inst Korea Struct Constr*. 2013;29(12):89-96.
17. Koo KM, Kim GY, Yoo JK, Lee EB. Properties of adiabatic temperature rise on concrete considering cement content and setting time. *Indian J Eng Mater Sci*. 2014;21(5):527-535.
18. Kong Q, Song G. A comparative study of the very early age cement hydration monitoring using compressive and shear mode smart aggregates. *IEEE Sensors J*. 2017;17(2):256-260.
19. Kong Q, Hou S, Ji Q, Mo YL, Song G. Very early age concrete hydration characterization monitoring using piezoceramic based smart aggregates. *Smart Mater Struct*. 2013;22(8):1-7.
20. Akram KJ, Ahmed A, Islam T. Fringing field impedance sensor for hydration monitoring and setting time determination of concrete material. *IEEE Trans Instrum Meas*. 2019;69(5):2131-2138.
21. Akram KJ, Ahmed A, Islam T. Fringing field impedance sensor for hydration monitoring and setting time determination of concrete material. *IEEE Trans Instrum Meas*. 2020;69(5):2131-2138.
22. Manchiryal RK, Neithalath N. Electrical property-based sensing of concrete: influence of material parameters on dielectric response. *Am Concr Institute, ACI Spec Publ*. 2008;23-40.
23. Manchiryal RK, Neithalath N. Analysis of the influence of material parameters on electrical conductivity of cement pastes and concretes. *Mag Concr Res*. 2009;61(4):257-270.
24. Jain S, Mishra PK, Thakare VV, Mishra J. Microstrip moisture sensor based on microstrip patch antenna. *Progress In Electromagnetics Research M*. 2018;76:177-185.
25. Ghretli MM, Khalid K, Grozescu IV, Sahri MH, Abbas Z. Dual-frequency microwave moisture sensor based on circular microstrip antenna. *IEEE Sensors J*. 2007;7(12):1749-1756.
26. Teng KH, Kot P, Muradov M, et al. Embedded smart antenna for non-destructive testing and evaluation (NDT&E) of moisture content and deterioration in concrete. *Sensors*. 2019;19(3):1-12.
27. Yi X, Cho C, Wang Y, Tentzeris MM. Battery-free slotted patch antenna sensor for wireless strain and crack monitoring. *Smart Struct Syst*. 2016;18(6):1217-1231.
28. Yi X, Wu T, Wang Y, Leon RT, Tentzeris MM, Lantz G. Passive wireless smart-skin sensor using RFID-based folded patch antennas. *Int J Smart Nano Mater*. 2011;2(1):22-38.
29. Zhang X, Ding XZ, Ong CK, Tan BTG, Yang J. Dielectric and electrical properties of ordinary Portland cement and slag cement in the early hydration period. *J Mater Sci*. 1996;31(5):1345-1352.
30. Fortaki T, Djouane L, Chebara F, Benghalia A. Radiation of a rectangular microstrip patch antenna covered with a dielectric layer. *Int J Electron*. 2008;95(9):989-998.
31. Bernhard JT, Tousignant CJ. Resonant frequencies of rectangular microstrip antennas with flush and spaced dielectric superstrates. *IEEE Trans Antennas Propag*. 1999;47(2):302-308.
32. Wakodkar RR, Gupta B, Chakraborty S. Variation of resonant frequency of a rectangular microstrip patch antenna due to accumulation of water over its surface. *Int Conf Appl Electromagn Student Innov Compet Award AEM2C 2010*. 2010;239-243.
33. Li Y, Bowler N. Resonant frequency of a rectangular patch sensor covered with multilayered dielectric structures. *IEEE Trans Antennas Propag*. 2010;58(6):1883-1889.
34. Shams KMZ, Ali M. Wireless power transmission to a buried sensor in concrete. *IEEE Sensors J*. 2007;7(12):1573-1577.
35. Yuan S, Lai X, Zhao X, Xu X, Zhang L. Distributed structural health monitoring system based on smart wireless sensor and multi-agent technology. *Smart Mater Struct*. 2006;15(1):1-8.
36. Huang H. Flexible wireless antenna sensor: a review. *IEEE Sensors J*. 2013;13(10):3865-3872.

37. Huang H, Chen ZN. Antenna sensors in passive wireless sensing systems. In: Chen ZN, ed. *Handbook of Antenna Technologies*. Springer; 2015:1-34.
38. McGee K, Anandarajah P, Collins D. A review of chipless remote sensing solutions based on RFID technology. *Sensors*. 2019;19(22): 1-51.
39. Hu J, Ma F, Wu S. Comprehensive investigation of leakage problems for concrete gravity dams with penetrating cracks based on detection and monitoring data: a case study. *Struct Control Health Monit*. 2018;25(4):1-18, e2127.
40. Zhu Y, Chen J, Zhang Y, Xiong F, He F, Fang X. Temperature tracer method for crack detection in underwater concrete structures. *Struct Control Health Monit*. 2020;27(9):1-12, e2595.
41. Li Z, He G, Wang S. NFRA-AIC: a RFID reader anti-collision protocol with adaptive interrogation capacity. *IEEE Access*. 2019;7:86493-86509.
42. Forouzandeh M, Karmakar NC. Chipless RFID tags and sensors: a review on time-domain techniques. *Wirel Power Transf*. 2015;2(2): 62-77.
43. Yao J, Tjuatja S, Huang H. Real-time vibratory strain sensing using passive wireless antenna sensor. *IEEE Sensors J*. 2015;15(8):4338-4345.
44. Xue S, Xu K, Xie L, Wan G. Crack sensor based on patch antenna fed by capacitive microstrip lines. *Smart Mater Struct*. 2019;28(8):1-13.
45. Xue S, Yi Z, Xie L, Wan G, Ding T. A passive wireless crack sensor based on patch antenna with overlapping sub-patch. *Sensors*. 2019; 19(19):1-14.
46. Yao J, Skilskyj J, Huang H. A compact, low-cost, real-time interrogation system for dynamic interrogation of microstrip patch antenna sensor. 10598.
47. Xue S, Yi Z, Xie L, et al. Double-frequency passive deformation sensor based on two-layer patch antenna. *Smart Struct Syst*. 2021;27(6): 969-982.
48. Becari W, Peres HEM, Falla MDPH, et al. Development of humidity sensors based on microstrip patch antenna with single walled carbon nanotubes. *Sens Lett*. 14:1123-1128.
49. Zhou S, Deng F, Yu L, Li B, Wu X, Yin B. A novel passive wireless sensor for concrete humidity monitoring. *Sensors*. 2016;16(9):1-15.
50. Yao J, Tchafa FM, Jain A, et al. Far-field interrogation of microstrip patch antenna for temperature sensing without electronics. *IEEE Sensors J*. 2016;16(19):7053-7060.
51. Tchafa FM, Huang H. Microstrip patch antenna for simultaneous strain and temperature sensing. *Smart Mater Struct*. 2018;27(6):1-16, 065019.
52. Aïtcin P-C. 2—Phenomenology of cement hydration. In: Aïtcin P-C, ed. *Science and Technology of Concrete Admixtures*. Woodhead Publishing:15-25.
53. Xu W, Li Q, Hu Y. Water content variations in the process of concrete setting. *Shuili Fadian Xuebao/Journal Hydroelectr Eng*. 2017;36: 92-103.
54. Taylor HF. *Cement Chemistry*. 2nd ed. Thomas Telford; 1997.
55. Pavlík J, Tydlitát V, Černý R, et al. Application of a microwave impulse technique to the measurement of free water content in early hydration stages of cement paste. *Cem Concr Res*. 2003;33(1):93-102.
56. Dirksen C, Dasberg S. Improved calibration of time domain reflectometry soil water content measurements. *Soil Sci Soc Am J*. 1993; 57(3):660-667.
57. Sun ZJ. Estimating volume fraction of bound water in Portland cement concrete during hydration based on dielectric constant measurement. *Mag Concr Res*. 2008;60(3):205-210.
58. Birchack JR, Gardner CG, Hipp JE, Victor JM. High dielectric constant microwave probes for sensing soil moisture. *Proc IEEE*. 1974; 62(1):93-98.
59. Shishir MDIR, Mun S, Kim HC, Kim JW, Kim J. Frequency-selective surface-based chipless passive RFID sensor for detecting damage location. *Struct Control Health Monit*. 2017;24(12):1-10, e2028.
60. General Administration of Quality Supervision, Inspection and Quarantine (AQSIQ) and Standardization Administration (SAC) of the People's Republic of China. GB/T 1346-2011 test methods for water requirement of normal consistency, setting time and soundness of the Portland cement, Standards Press of China, https://www.chinesestandard.net/PDF/English.aspx/GBT1346-2011
61. Yadav RK, Yadava RL. Superstrate loaded rectangular microstrip patch antennas—an overview. *J of Information, Intelligence, and Knowledge*. 2011;3(2):107-124.

How to cite this article: Yi Z, Xue S, Xie L, Wan G. Detection of setting time in cement hydration using patch antenna sensor. *Struct Control Health Monit*. 2021;e2855. doi:10.1002/stc.2855